inter.noise
21-24 AUGUST
SCOTTISH EVENT CAMPUS
GLASGOW 2022

A Preliminary Investigation of an Active Membrane-type Acoustic Metamaterial

Felix Langfeldt[1]
Institute of Sound & Vibration Research, University of Southampton
University Road, Highfield, Southampton, SO17 1BJ, United Kingdom

Jordan Cheer[2]
Institute of Sound & Vibration Research, University of Southampton
University Road, Highfield, Southampton, SO17 1BJ, United Kingdom

ABSTRACT

One of the most promising features of membrane-type acoustic metamaterials (MAM) is their anti-resonance at low frequencies, which typically exhibits sound transmission loss values that can significantly exceed the corresponding mass-law values. The bandwidth of this anti-resonance, however, is usually very small, which limits the applicability of MAM in practical noise control problems. In previous research it has been shown that different types of actuators (e.g. magnets, electrodes, or pressurized air) can be used to adjust the anti-resonance frequency of MAM, for example to adapt to changing tonal frequencies. However, these actuation principles require additional components to be added to the otherwise lightweight MAM. To overcome these limitations, this paper will present preliminary results from an experimental study of a smart MAM which has the sensors and actuators compactly embedded within the added mass located at the center of the membrane of the unit cell. A small accelerometer is used to measure the vibration of the added mass and this signal is fed back to a controller, which is used to actuate the MAM using a small electrodynamic exciter. An impedance tube is used to measure the sound transmission through the smart MAM and different control algorithms are compared.

1. INTRODUCTION

Membrane-type acoustic metamaterials (MAM) are composed of a planar periodic array of sub-wavelength sized unit cells, where each unit cell consists of a thin flexible membrane with at least one added mass attached to the membrane. Essentially, this arrangement forms a resonant spring-mass system that, when tuned properly, can exhibit so-called anti-resonances at low frequencies with sound transmission loss values much higher than expected from the mass-law [1, 2]. Due to their compact design, MAM can be designed to be very lightweight and therefore are a very attractive potential solution for low-frequency tonal noise control, especially when weight and volume of acoustic treatments are highly constrained (such as in aircraft, vehicles, or mobile sound barriers). While these properties of MAM are encouraging, the low bandwidth of the anti-resonance frequencies limits their applications to noise sources with very narrowband noise or stationary tones. Certain approaches for improving the bandwidth of MAM have been suggested in previous research, for example by stacking

[1] F.Langfeldt@soton.ac.uk
[2] J.Cheer@soton.ac.uk

multiple layers of MAM or coupling unit cells with different anti-resonance frequencies in parallel [3, 4]. These approaches, however, ultimately lead to more complex, heavier, and bulkier structures. Also, the peak noise reduction performance will be reduced when increasing the bandwidth using passive means, which reduces the advantage of MAM over conventional partitions governed by the mass-law.

On the other hand, an active actuation of the MAM could be employed to adjust the anti-resonances according to the incident noise spectrum. For example, Xiao *et al.* [5] investigated changing the anti-resonance frequency of a MAM unit cell by applying an electric field, essentially changing the stiffness of the resonant spring-mass system using voltages of up to 1 kV. In Ref. [6], a non-electrical approach for achieving similar anti-resonance frequency shifts by employing a static pressurization of the MAM has been demonstrated. These actuation principles clearly can be employed to actively adjust the acoustical properties of MAM, but they require additional structures (e.g. electrodes, as in Ref. [5], or pressure tubes, as in Ref. [6]) which add to the weight and complexity of these MAM. Furthermore, feedback control algorithms and many adaptive filtering methods, such as the well-known filtered-reference least mean squares algorithm (FxLMS), require error sensors (typically microphones) to be positioned as close to the receiver as possible [7].

A more integral approach that could help minimizing the weight and complexity of active MAM would be to embed both actuators and sensors within the added mass which is required anyway for the desired functionality of MAM. Instead of using microphones, which—depending on the environmental conditions—could deteriorate after some time, accelerometers on the surface of the MAM could be used as a more robust alternative to estimate the error signals at the receiver location using the remote sensing technique [8].

In this contribution, the results of a preliminary investigation of an active MAM with a compact sensor-actuator added mass will be presented. The basic components of one unit cell of the active MAM and the active control algorithms will be discussed in Section 2. In Section 3, simulations will be performed to estimate the performance of the active MAM using different control strategies. Based on these results, an experimental test sample has been built and measured inside an impedance tube. The experimental results are presented in Section 4. Finally, Section 5 concludes the paper with a brief summary of the results.

2. SET-UP OF THE ACTIVE MAM

2.1. Membrane-type acoustic metamaterial

Since the measurements were to be conducted inside a circular impedance tube, the shape of the unit cell of the MAM considered here is circular. It should be noted that rectangular MAM unit cells are more suitable for covering large surfaces with multiple unit cells, but there are no fundamental differences between the vibro-acoustic behaviour of circular and rectangular MAM [9]. The results presented herein can therefore be readily transferred to MAM with rectangular unit cells.

The diameter of the MAM unit cell is $D = 84\,\mathrm{mm}$. The membrane is a 55 µm thick PET film with a pretension[1] of $220\,\mathrm{N\,m^{-1}}$. The shape of the added mass is cylindrical, with a diameter of $D_\mathrm{M} = 60\,\mathrm{mm}$ and a thickness of $h_\mathrm{M} = 2\,\mathrm{mm}$. The material of the added mass is acrylic glass. All material parameters, as used in the simulation model, are provided in Table 1. The resulting surface

[1]The pretension of the membrane has been determined indirectly by measuring the fundamental frequency of the unloaded membrane (i.e. without added mass, actuator, and sensor) and adjusting the pretension in a simulation model of the membrane to match the measured fundamental frequency.

Table 1: Material parameters of the MAM components.

	Membrane	Mass	
Material	PET	Acrylic glass	
Density	1310	1190	$\mathrm{kg\,m^{-3}}$
Young's modulus	2.3	3.2	GPa
Poisson's ratio	0.4	0.35	—
Loss factor	10	0	%

mass density of the baseline MAM (without sensor and actuator) is $1.3\,\mathrm{kg\,m^{-2}}$.

2.2. Actuator and sensor

For the preliminary study in this contribution, the actuation of the MAM is performed using a miniature electrodynamic exciter attached to the top surface of the added mass. An electrical input signal can be used to drive a moving mass M_{ms} with a voice coil inside the exciter and thus impose a dynamic force on the MAM. In this work, a type TEAX09C005-8 exciter from Tectonic Audio Labs was used, which is very compact ($26\,\mathrm{mm} \times 13\,\mathrm{mm} \times 6.5\,\mathrm{mm}$) and lightweight ($M_{\mathrm{exc}} = 3.2\,\mathrm{g}$) and therefore well suited for the purposes of this investigation. The relevant Thiele/Small parameters of the exciter have been determined systematically in previous work [10] and the values provided in Table 2 will be used for modelling the electrodynamic behaviour of the exciter.

The acceleration of the MAM unit cell center is measured using a PCB Piezotronics type 352A24 miniature accelerometer. The sensor is attached to the MAM on the underside of the membrane and is very small in size ($10\,\mathrm{mm} \times 7\,\mathrm{mm} \times 5\,\mathrm{mm}$), with a weight of only $M_{\mathrm{acc}} = 0.8\,\mathrm{g}$. Taking into account the additional mass introduced by the exciter and the accelerometer, the surface mass density of the active MAM is approximately $2\,\mathrm{kg\,m^{-2}}$.

2.3. Active control algorithms

In this work, two active control algorithms for increasing the sound reduction of the active MAM will be investigated. The first algorithm is a feedback loop, where the error signal is passed through a controller C, which generates a voltage signal U that is provided to the exciter. In typical active noise control applications, the error signal is provided by a microphone measuring the transmitted sound pressure p_{t}. A schematic representation of this setup is shown on the left side of Fig. 1. The second algorithm investigated here is an adaptive feedforward filter based on the FxLMS method [7]. A schematic setup of this active noise control method using the measured pressure as the error signal is shown in Fig. 2 (left side). The LMS block represents the algorithm for updating the filter coefficients $\mathbf{w}$ of the adaptive filter F based on the error signal $e = p_{\mathrm{t}}$ and the reference signal r filtered by a model

Table 2: Mechanical and electrical parameters for the type TEAX09C005-8 exciter.

M_{exc}	M_{ms}	D_{ms}	C_{ms}	L_{e}	R_{e}	$B\ell$
3.2 g	3.07 g	$830\,\mathrm{kg\,s^{-1}}$	$0.23\,\mathrm{mm\,N^{-1}}$	0.17 mH	$8.8\,\Omega$	1.6 T m

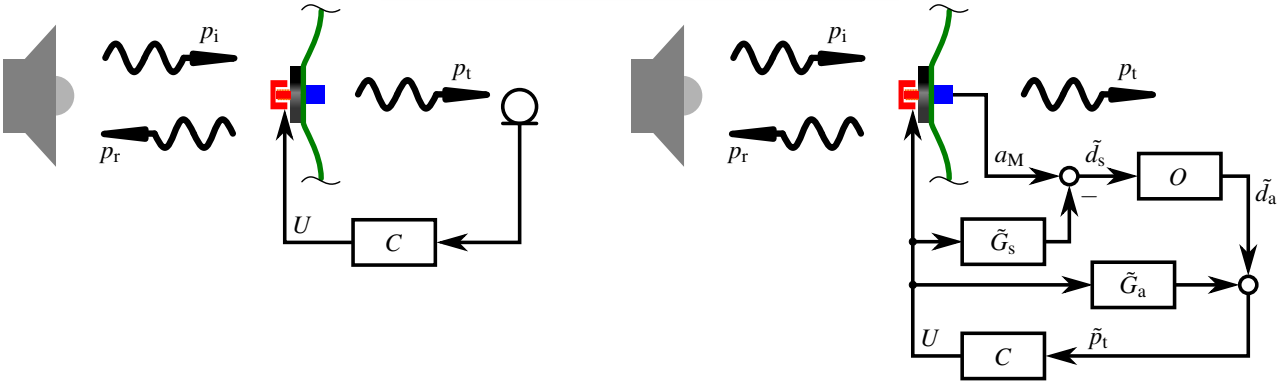

Figure 1: Schematic representation of the transmitted pressure feedback control algorithm. Left: Direct measurement of p_t using a microphone; Right: Remote sensing technique based on the mass acceleration a_M.

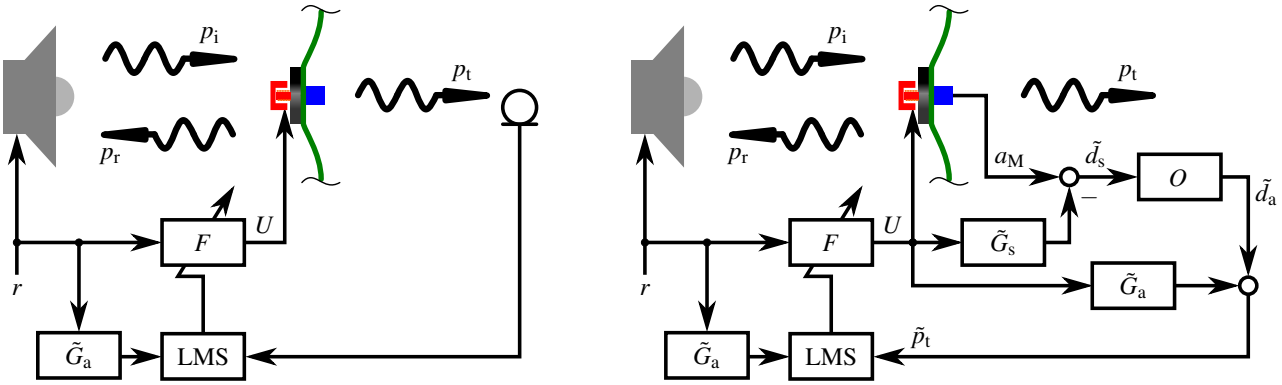

Figure 2: Schematic representation of the FxLMS adaptive feedforward control algorithm. Left: Direct measurement of p_t using a microphone; Right: Remote sensing technique based on the mass acceleration a_M.

of the plant response $\tilde{G}_a$. The equation used in updating the filter coefficients is

$$\mathbf{w}_n = \mathbf{w}_{n-1} + \mu e_n \frac{\tilde{\mathbf{r}}_n}{\|\tilde{\mathbf{r}}_n\|^2}, \tag{1}$$

where μ is a convergence parameter and $\tilde{\mathbf{r}}$ is the filtered reference signal.

2.4. Remote sensing technique

In this investigation, the error microphone that measures p_t is replaced by an accelerometer mounted on the surface of the MAM measuring the acceleration of the added mass a_M. Therefore, in order to control the transmitted sound pressure using the algorithms presented in the previous sub-section, p_t needs to be extrapolated based on the measured acceleration. The remote sensing technique [8] will be used for this purpose. The physical background of this method is briefly outlined below.

The transmitted pressure p_t is given by the superposition of the disturbance d_a from the acoustic path through the MAM and the sound radiated by the MAM vibration induced by the exciter (acoustical plant response G_a):

$$p_t = d_a + G_a U. \tag{2}$$

In the same way, the acceleration of the mass a_M depends on the structural disturbance d_s and the structural plant response G_s:

$$a_\mathrm{M} = d_\mathrm{s} + G_\mathrm{s} U. \tag{3}$$

Since a_M is measured, the structural disturbance can be estimated using a plant model $\tilde{G}_\mathrm{s}$:

$$d_\mathrm{s} \approx \tilde{d}_\mathrm{s} = a_\mathrm{M} - \tilde{G}_\mathrm{s} U. \tag{4}$$

In order to be able to estimate the transmitted pressure p_t, it follows from Eq. (2) that the acoustical disturbance d_a must be known. Using a so-called observation filter O, the acoustical disturbance can be estimated from the structural disturbance as follows:

$$\tilde{d}_\mathrm{a} = O \tilde{d}_\mathrm{s}. \tag{5}$$

Thus, combining Eqs. (2), (4), and (5) yields the following equation for estimating the transmitted sound pressure based on the measured acceleration and the plant response:

$$\tilde{p}_\mathrm{t} = \tilde{d}_\mathrm{a} + \tilde{G}_\mathrm{a} U = O a_\mathrm{M} + \left(\tilde{G}_\mathrm{a} - O \tilde{G}_\mathrm{s}\right) U. \tag{6}$$

The right sides in Figs. 1 and 2 illustrate how the remote sensing technique has been implemented in case of the feedback control and the FxLMS adaptive feedforward control, respectively.

3. NUMERICAL INVESTIGATION

3.1. Numerical setup

All simulations have been performed in the frequency domain for the frequency range $f = 50\,\mathrm{Hz} - -1600\,\mathrm{Hz}$. The mesh and boundary conditions used for the finite element method (FEM) simulations of the active MAM are shown in Fig. 3. Since both the exciter as well as the accelerometer are small compared to the acoustic wavelengths within the frequency range of interest, it can be assumed that their interaction with the acoustic field is negligible. Therefore, these components have been coupled with the MAM using points so that the whole MAM unit cell and surrounding fluid domains can be

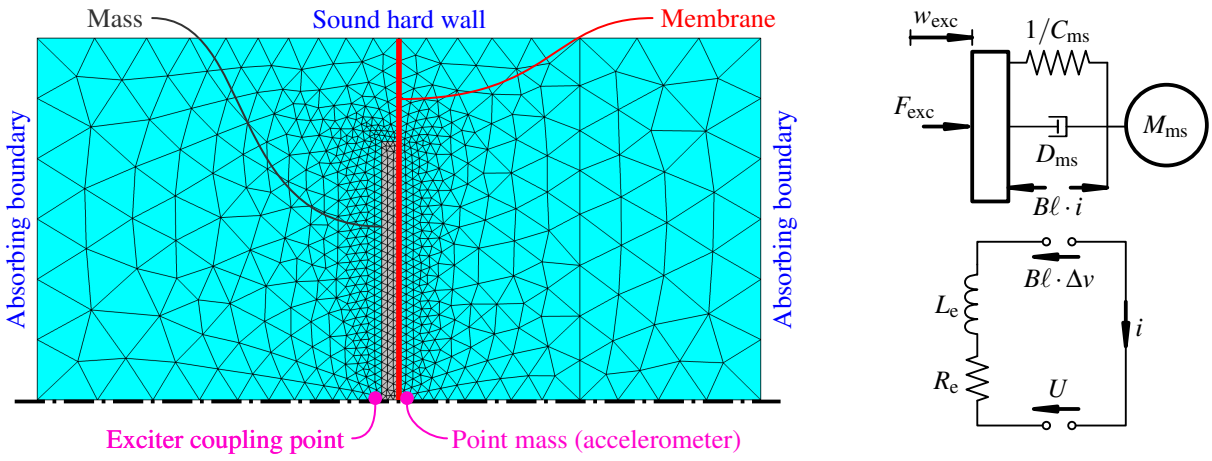

Figure 3: Left: Mesh and boundary conditions in the axisymmetric FEM simulation model of the active MAM; Right: Lumped electro-mechanical model of the exciter.

modelled using a two-dimensional axisymmetric model. The fluid and the mass have been discretized using quadratic triangular elements. The membrane is modelled using quadratic one-dimensional shell elements, including the uniform in-plane membrane pretension.

The exciter was modeled using a lumped representation of the electrical and mechanical parts (as shown in Fig. 3), with the lumped element parameters given in Table 2. This model was coupled to the FEM model of the MAM at the exciter coupling point in the centre of the added mass by enforcing the continuity of force F_{exc} and displacement w_{exc} of the exciter base and the added mass at this point. In order to include the additional mass of the accelerometer in the model, the accelerometer is represented by a point mass M_{acc}.

3.2. Simulation results

First, simulation results for the feedback control setup will be presented. Fig. 4(a) shows the simulated transmission loss TL of the active MAM using the transmitted pressure p_{t} as the error signal and a positive gain K as the controller C. To make sure that the feedback loop is stable, the magnitude of the gain K has been increased in small increments until either the gain margin or the phase margin of the open loop response become almost zero. Thus, the simulation results represent the upper limit on what can be achieved within the stability limits of the active MAM.

In case of no control ($K = 0$), the TL spectrum of the MAM exhibits two peaks: The first peak at approximately 185 Hz corresponds to the mechanical resonance frequency of the exciter [10]. The second peak at 700 Hz with much higher TL values is the anti-resonance of the MAM. By increasing the value of the gain K, the TL between the two peaks can be increased, leading to a broad plateau-like curve that enhances the bandwidth of the MAM. It should be noted that for $K \geq 20\,\mathrm{mV\,Pa^{-1}}$ the TL of the MAM becomes negative around the first resonance frequency at 100 Hz, because the sound radiated by the excitation using the exciter superimposes constructively with the transmitted sound. One way to avoid this is to use a suitable filter that reduces the output signal of the controller in this frequency range.

The simulation results for the active MAM with the acceleration of the mass a_{M} being used as the error signal are shown in Fig. 4(b). Since for sound radiation problems acoustic pressure and structural velocity are directly linked, the feedback controller was simulated as an integrator with $C = K/s$ (where $s = \mathrm{i}2\pi f$ is the Laplace variable), in order to estimate the mass velocity v_{M} from the measured acceleration signal. The results in Fig. 4(b) indicate that the mass velocity feedback leads

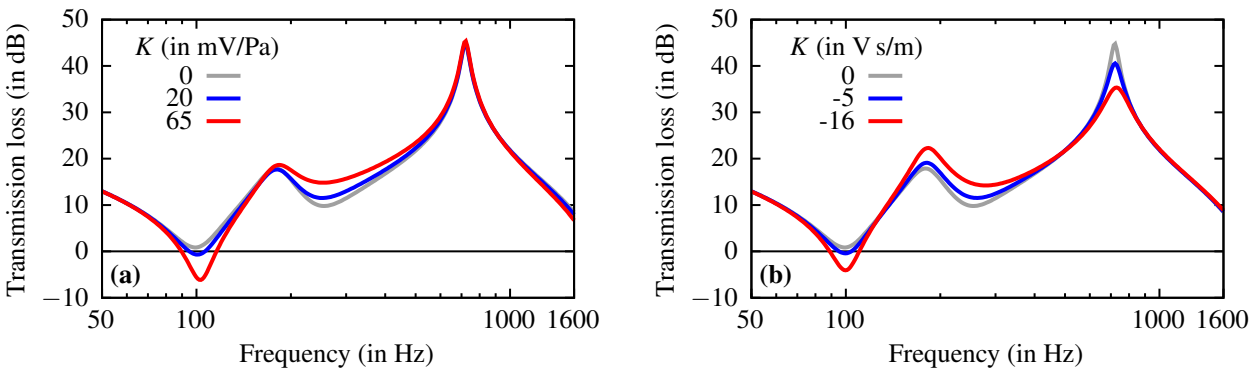

Figure 4: Simulation results for the active MAM with different feedback control methods. (a) Transmitted pressure p_{t} feedback; (b) Added mass velocity v_{M} feedback.

to an increase in the maximum TL at the exciter resonance as the magnitude of the negative feedback gain K is increased. However, the second peak is reduced at the same time, leading to a reduced noise insulation performance at the MAM anti-resonance. This is contrary to what has been observed in the case of the pressure feedback.

Next, it will be investigated how the FxLMS adaptive control algorithm will affect the transmission loss of the active MAM when a_M is used as the error signal, instead of p_t.[2] To get an estimate of the (theoretically possible) best-case performance, the filter F is assumed to correspond to the ideal filter $F = -H_\mathrm{s}/G_\mathrm{s}$ (with H_s being the structural response of the MAM due to acoustic excitation), such that $a_\mathrm{M} = 0$. The simulation results for this case are shown in Fig. 5. It can be seen that if FxLMS is used to eliminate the acceleration of the mass, the sound transmission loss of the MAM changes fundamentally. The first resonance frequency is increased from 100 Hz to almost 700 Hz, leading to a significantly reduced sound transmission loss within the frequency range where the anti-resonance frequency of the passive MAM is. At lower frequencies, the TL of the active MAM becomes stiffness-controlled, which could be regarded as an improvement over the passive MAM performance at very low frequencies. However, this stiffness-controlled TL behaviour cannot be achieved in practice, because the ideally fixed boundary conditions assumed in the simulations will not be representative for large-scale MAM panels containing multiple unit cells [11]. The displacement shapes of the simulated active MAM shown in Fig. 5 for two characteristic frequencies (660 Hz: first resonance frequency; 975 Hz: first anti-resonance frequency) show how the mass is essentially clamped at the accelerometer attachment point in the center of the mass and the membrane and mass are bending around this point. This explains why the active MAM becomes much stiffer when the mass acceleration at the accelerometer attachment point is controlled.

In summary, the simulation results for the accelerometer-based FxLMS configuration show that—even when an ideal filter can be identified using FxLMS—using the mass acceleration as the error signal will not provide an improvement of the sound insulation bandwidth of the MAM. Therefore, it can be expected that by using the remote sensing technique the sound transmission loss of the active MAM can be clearly improved.

[2] Simulations of the FxLMS configuration with a pressure-based error signal have not been performed, because in that case an ideal filter F would lead to $p_\mathrm{t} = 0$ for all frequencies and, consequently, TL $\to \infty$.

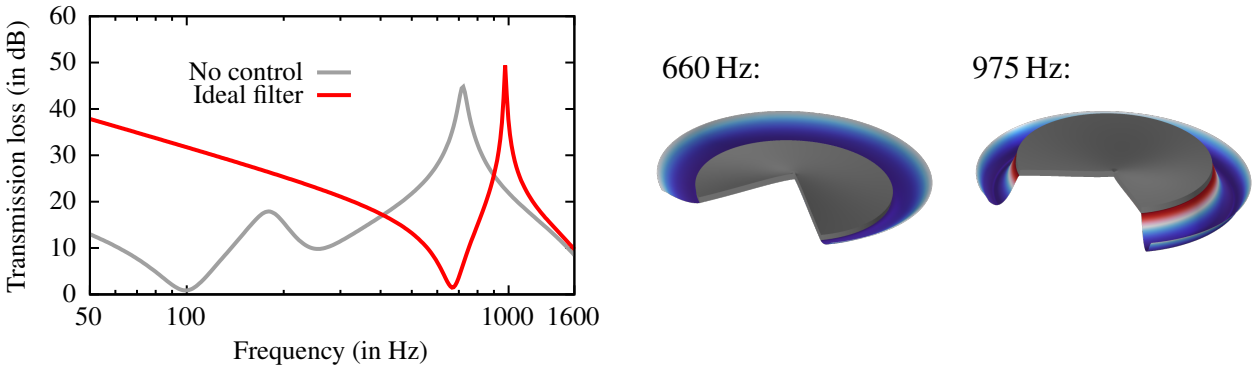

Figure 5: Simulation results for the active MAM with an ideal filter F that sets the acceleration at the accelerometer attachment point to zero. Left: Sound transmission loss; Right: Simulated deformation at two characteristic frequencies.

4. IMPEDANCE TUBE MEASUREMENTS

4.1. Measurement setup

The MAM unit cell was manufactured by clamping a PET film in a circular sample holder and pre-tensioning the film using a heat gun. The added mass disc, exciter, and accelerometer were fixed in position using adhesives, ensuring good mechanical coupling between all components. Fig. 6 shows photographs of the experimental test sample.

The MAM sample was placed inside a 100 mm diameter impedance tube, as illustrated in Fig. 7. The ends of the tube were terminated using sound absorbing materials to minimize reflections. On each side of the MAM, two microphones were used to estimate the amplitudes of the waves propagating in both directions in front of the MAM (A and B) and behind the MAM (C and D) [12]. These wave amplitudes have been used in the post-processing of the measurements to estimate the TL of the MAM according to

$$\mathrm{TL} \approx -20\lg\left|\frac{C}{A}\right|. \tag{7}$$

All microphone signals and the accelerometer signal were connected to a dSPACE DS-1103 data acquisition system. The DS-1103 also provided the electrical signals for the loudspeaker and the exciter attached to the MAM. These output signals have been low-pass filtered and amplified before being fed into the loudspeaker or exciter. The source signal to the loudspeaker was band-limited white noise throughout the experiment.

The active control algorithms have been implemented using a real-time interface with SIMULINK. The sampling rate was 4000 Hz, so that the frequency range of interest (50 Hz–1600 Hz) could be captured accurately. To measure the transmitted pressure p_t, the signal of microphone #3 was used which was located at a distance of $d_\mathrm{mic} = 200\,\mathrm{mm}$ away from the MAM. The plant models $\tilde{G}_\mathrm{a}$ and $\tilde{G}_\mathrm{s}$ as well as the observation filter O have been implemented as finite impulse response (FIR) filters with 200 coefficients. These coefficients have been estimated using the LMS method before the actual measurements of the closed loop responses had been conducted.

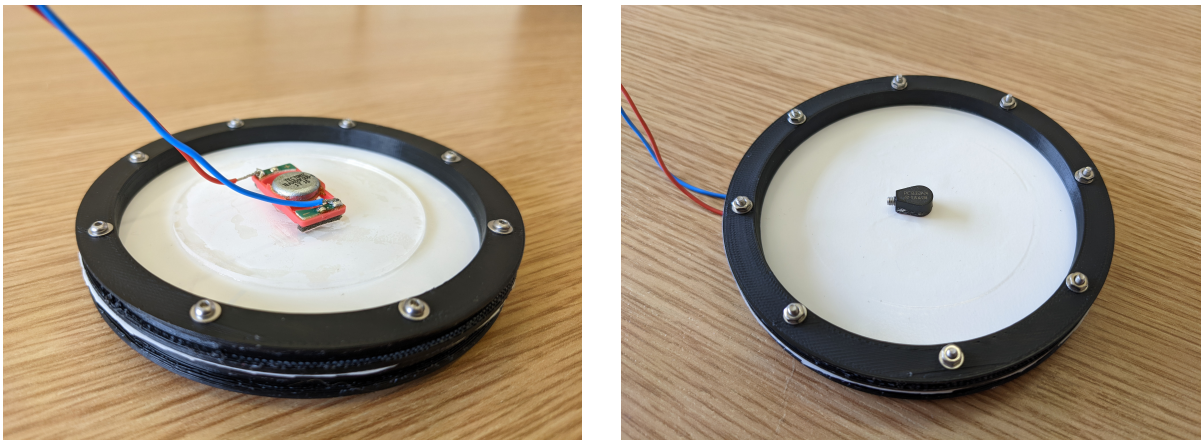

Figure 6: Experimental test sample of the active MAM. Left: Top side with added mass and exciter; Right: Bottom side with accelerometer.

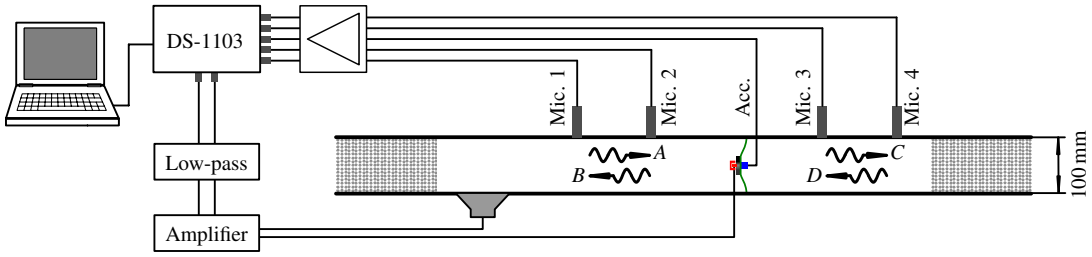

Figure 7: Illustration of the impedance tube measurement set-up.

4.2. Measurement results

In order to verify the overall accuracy of the numerical model, the measured and simulated transmission loss of the passive MAM are compared in Fig. 8. In general, the agreement between simulation and experiment is reasonably good, in particular the characteristic shape of the TL spectrum with the two peaks is clearly visible in both cases. It should be highlighted that the measured anti-resonance frequency is slightly lower than in the simulations. It is possible that by pressing the sample holder inside the impedance tube the membrane pretension was reduced slightly, leading to the lower anti-resonance frequency. Furthermore, additional peaks can be seen in the experimental results (for example between 300 Hz and 400 Hz) which may be the result of slight asymmetries present in the experimental test sample that the axisymmetric numerical model cannot take into account.

The measurement results for the feedback control loops are shown in Fig. 9. During the measurements, the magnitude of the feedback gain has been gradually increased in each configuration until the feedback loop became unstable. The actual measurement data was then acquired for a slightly lower feedback gain magnitude to demonstrate what is possible using these active control concepts without further stabilization measures. Fig. 9(a) shows a comparison of the MAM sound transmission loss with feedback of the transmitted pressure p_t. The solid blue line represents results obtained with a direct measurement of p_t using a microphone and the dotted line corresponds to the remote sensing technique. A comparison with the simulated prediction of the feedback configuration in Fig. 4(a) shows that the overall gain in low-frequency transmission loss (up to about 6 dB) is similar to the simulations. Also, the MAM anti-resonance at approximately 700 Hz is mostly unaffected by the feedback (as in the simulations). However, some qualitative differences can be seen: The measure-

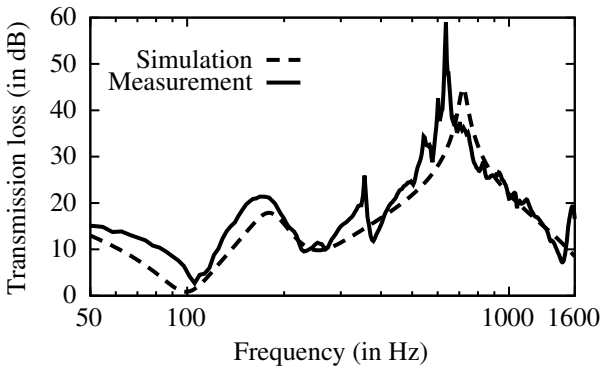

Figure 8: Comparison of the simulated and measured transmission loss for the passive MAM.

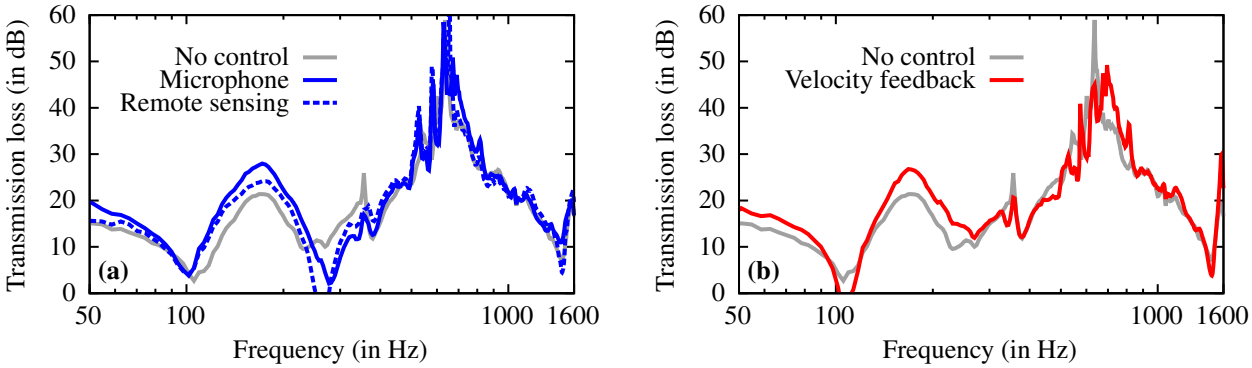

Figure 9: Measurement results for the active MAM with different feedback control methods. (a) Transmitted pressure p_t feedback (direct measurement and remote sensing technique); (b) Added mass velocity v_M feedback.

ments indicate a reduced TL at around 300 Hz, which was not predicted by the simulations. Further investigations are required to determine the explanation for this difference. When comparing the experimental results for the direct measurement of p_t and the remote sensing technique it can be seen that the remote sensing method is capable of replicating qualitatively the TL curve obtained for the microphone signal feedback. The TL improvement is not as high as in the direct measurement case, because the maximum feedback gain (before instability of the feedback loop) was 25 % lower in the remote sensing approach, hence the reduced performance. The lower stability margin requires further investigation, although it may be related to the controller relying on the signal estimated via the observation filter.

The experimental results for the mass velocity feedback are provided in Fig. 9(b). In this case, the measured data agrees well with the simulation results in Fig. 4(b): The TL is enhanced by up to 5 dB at the mechanical resonance frequency of the exciter, while a reduction of the peak TL at the MAM anti-resonance can be observed.

The measurements of the FxLMS-based active control configurations were performed with an adaptive filter F with 100 filter coefficients and the LMS convergence parameter set to $\mu = 0.1$. In Fig. 10(a), the experimental results for using the transmitted pressure as the error signal (either by using a microphone or the remote sensing technique) are shown. In general, the adaptive filter leads to a very broad frequency range with the transmission loss of the MAM exceeding 30 dB between 100 Hz and 1 kHz, substantially improving the bandwidth of the MAM. Imperfections in the noise cancelling performance can be attributed to the finite filter length and inaccuracies in the plant model. The remote sensing technique also leads to a very broad noise insulation band, however, with lower TL values compared to using the microphone-based error signals. Compared to the TL of the passive MAM, particularly at low frequencies, this still is a substantial improvement and demonstrates that the remote sensing technique can provide a reasonable replacement of an error microphone for active MAM.

Finally, the measurement results for the FxLMS algorithm using the mass acceleration as the error signal are shown in Fig. 10(b). As expected from the simulations, this does not lead to a broad improvement of the MAM transmission loss. Instead, the anti-resonance frequency is shifted due to the constrained motion of the added mass. It is noteworthy, though, that in the measurements shown here, the MAM anti-resonance frequency is reduced substantially (to 140 Hz), while the simulations

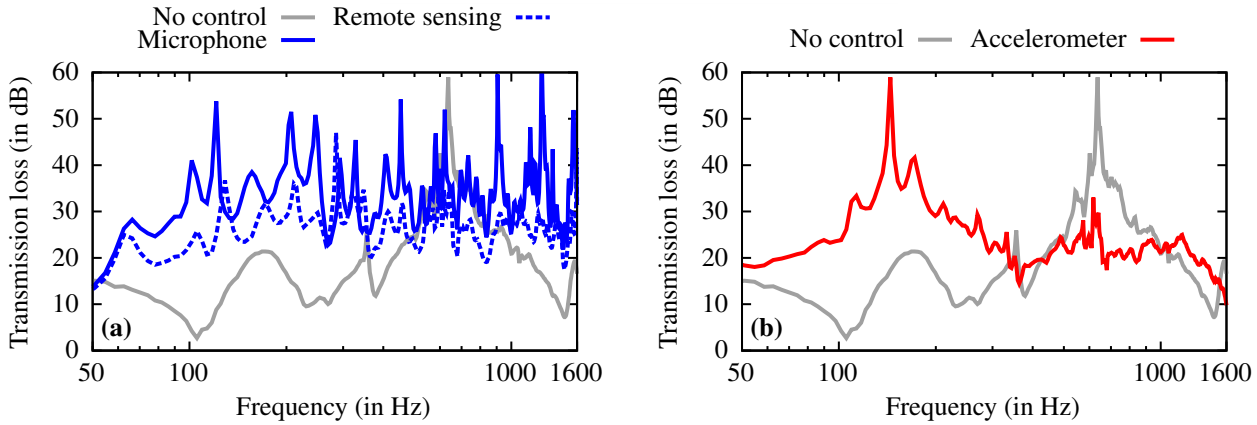

Figure 10: Measurement results for the active MAM with FxLMS adaptive feedforward control using different error signals. (a) Transmitted pressure p_t (direct measurement and remote sensing technique); (b) Added mass acceleration a_M.

predicted an increase of the anti-resonance frequency (see Fig. 5). The reason for this difference is still an open question. A reasonable assumption is that this could be related to the boundary conditions of the impedance tube test sample which will not be as perfectly fixed as assumed in the numerical model.

5. CONCLUSIONS

In this contribution a preliminary investigation of an active MAM based on numerical simulations and impedance tube measurements has been presented. The key innovation of the active MAM presented here was to use an accelerometer mounted directly on the surface of the MAM to estimate the transmitted sound pressure (using the remote sensing technique), which can be used as an error signal in active noise control algorithms. The actuation of the MAM was achieved using a small electrodynamic exciter attached to the added mass of the MAM.

Two active control strategies have been studied numerically and experimentally: A feedback loop using the transmitted pressure or the mass velocity could be demonstrated to improve the transmission loss of the MAM, especially at lower frequencies. Due to stability constraints of the feedback loops, this improvement was limited to around 5 dB–6 dB. More significant and much broader improvements could be achieved using the FxLMS adaptive feedforward control method, in particular when the transmitted pressure is used as the error signal. The remote sensing technique exhibited a promising performance in replicating the results from using a real error microphone.

6. ACKNOWLEDGEMENTS

F. Langfeldt's research was funded by the Deutsche Forschungsgemeinschaft (DFG, German Research Foundation) in the framework of the Walter Benjamin Programme (grant no. 455631459).

7. REFERENCES

1. Yang, Z., Mei, J., Yang, M., Chan, N. H. & Sheng, P. Membrane-Type Acoustic Metamaterial with Negative Dynamic Mass. *Physical Review Letters* **101,** 204301 (2008).

2. Naify, C. J., Chang, C.-M., McKnight, G. & Nutt, S. Transmission Loss and Dynamic Response of Membrane-Type Locally Resonant Acoustic Metamaterials. *Journal of Applied Physics* **108,** 114905 (2010).
3. Naify, C. J., Chang, C.-M., McKnight, G. & Nutt, S. R. Scaling of Membrane-Type Locally Resonant Acoustic Metamaterial Arrays. *The Journal of the Acoustical Society of America* **132,** 2784–92 (2012).
4. Langfeldt, F., Gleine, W. & von Estorff, O. An Efficient Analytical Model for Baffled, Multi-Celled Membrane-Type Acoustic Metamaterial Panels. *Journal of Sound and Vibration* **417,** 359–375 (2018).
5. Xiao, S., Ma, G., Li, Y., Yang, Z. & Sheng, P. Active Control of Membrane-Type Acoustic Metamaterial by Electric Field. *Applied Physics Letters* **106,** 091904 (2015).
6. Langfeldt, F., Riecken, J., Gleine, W. & von Estorff, O. A Membrane-Type Acoustic Metamaterial with Adjustable Acoustic Properties. *Journal of Sound and Vibration* **373,** 1–18 (2016).
7. Elliott, S. J. *Signal Processing for Active Control* (Academic Press, London, 2001).
8. Cheer, J. & Daley, S. Active Structural Acoustic Control Using the Remote Sensor Method. *Journal of Physics: Conference Series* **744,** 012184 (2016).
9. Langfeldt, F., Gleine, W. & von Estorff, O. Analytical Model for Low-Frequency Transmission Loss Calculation of Membranes Loaded with Arbitrarily Shaped Masses. *Journal of Sound and Vibration* **349,** 315–329 (2015).
10. Singleton, L., Cheer, J. & Daley, S. A Robust Optimised Shunted Electrodynamic Metamaterial for Multi-Mode Vibration Control. *Journal of Sound and Vibration* **527,** 116861 (2022).
11. Peiffer, A., Grünewald, M. & Lempereur, P. Comment on "a Lightweight yet Sound-Proof Honeycomb Acoustic Metamaterial" [Appl. Phys. Lett. 106, 171905 (2015)]. *Applied Physics Letters* **107,** 216101 (2015).
12. Song, B. H. & Bolton, J. S. A Transfer-Matrix Approach for Estimating the Characteristic Impedance and Wave Numbers of Limp and Rigid Porous Materials. *The Journal of the Acoustical Society of America* **107,** 1131–1152 (2000).